Materials Science in Semiconductor Processing 188 (2025) 109185

Contents lists available at ScienceDirect

Materials Science in Semiconductor Processing

journal homepage: www.elsevier.com/locate/mssp

Comprehensive DFT study of $ZnGe_{1-x}Si_xAs_2$ alloys: Insights into structural, electronic, optical, and thermoelectric properties

S. Bougaa [a,b], H. Baaziz [c,d,*], T. Ghellab [c,d], S. Adalla [a,b], L. Bouhdjer [a,b], Ş. Uğur [e], G. Uğur [e], Z. Charifi [c,d]

[a] Department of Physics, Faculty of Sciences and Applied Sciences, University of Bouira, 10000, Bouira, Algeria
[b] Laboratory of Material Physics and Optoelectronic Compounds, University of Bouira, Algeria
[c] Department of Physics, Faculty of Science, University of M'sila, 28000, M'sila, Algeria
[d] Laboratory of Physics and Chemistry of Materials, University of M'sila, Algeria
[e] Department of Physics, Faculty of Science, Gazi University, 06500, Ankara, Turkey

ARTICLE INFO

Keywords:
Chalcopyrite alloys
Optoelectronic
Semiconductor
Thermoelectric properties

ABSTRACT

The substitution of Ge with Si in the $ZnGeAs_2$ chalcopyrite semiconductor and its impact on structural, electronic, optical, and thermoelectric properties have been systematically studied using density functional theory. This study demonstrates the tunability of material properties through alloying, revealing novel insights into the $ZnGe_{1-x}Si_xAs_2$ ($x = 0–1$) system. The exchange-correlation energy was evaluated using the local density, generalized gradient, and modified Becke-Johnson schemes, ensuring accurate predictions. The calculated structural parameters and band gap energies for $ZnGeAs_2$ and $ZnSiAs_2$ exhibit excellent agreement with experimental data, validating the reliability of our approach.

Both $ZnGeAs_2$ and $ZnSiAs_2$ exhibit semiconductor characteristics with a direct band gap at the Γ point, making them promising for optoelectronic applications. The alloys show anisotropic optical behavior, with $ZnGe_{0.25}Si_{0.75}As_2$ demonstrating the highest refractive index and energy loss, making it a strong candidate for UV-shielding and optoelectronic devices. Thermoelectric analysis identifies $ZnGe_{0.75}Si_{0.25}As_2$ as the optimal composition, achieving a maximum Seebeck coefficient of 228.26 μV/K at 800 K. Moreover, by tuning the carrier concentration to $n = 4.87 \times 10^{18}$ cm^{-3}, the Seebeck coefficient can be significantly enhanced to 449.44 μV/K. These findings highlight the potential of Si substitution to enhance material performance and provide a roadmap for tailoring the structural, optical, and thermoelectric properties of chalcopyrite semiconductors.

1. Introduction

The rapid advancements in renewable energy technologies have amplified the need for high-performance materials with tailored properties for specific applications. Among these, chalcopyrite compounds have emerged as some of the most promising materials, primarily due to their remarkable electrical, optical, and thermoelectric properties [1]. These properties make chalcopyrites highly versatile, enabling their use in various technological domains, including photovoltaic detectors, multijunction solar cells, light-emitting diodes (LEDs), modulators, and nonlinear optics [2–5]. Furthermore, their tunable band gaps position them as excellent candidates for infrared detectors, opening avenues for their use in optoelectronics and energy harvesting applications [6].

Within the ternary chalcopyrite family, compounds with the general formula A-B-C_2 (where A = Mg, Zn, Cd; B = Si, Ge, Sn; C = P, As, Sb) have gained significant attention due to their direct band gaps and highly adjustable properties. In particular, pnictide-based chalcopyrites like $ZnGeAs_2$ and $ZnSiAs_2$ stand out for their favorable electronic and optical behaviors. Their ability to balance good electronic conductivity with low thermal conductivity further enhances their potential for thermoelectric applications, especially in energy conversion and waste heat recovery systems.

Significant progress has been made in the study of these materials through both experimental and theoretical approaches. Experimentally, $ZnGeAs_2$ has been investigated for its structural and optoelectronic properties by Drahokoupil et al. [7], Solomon et al. [8], and Shah et al. [9], while related compounds such as $ZnSiAs_2$, $ZnGeP_2$, and $CdGeP_2$ have been explored by Masumoto et al. [10]. On the theoretical front,

* Corresponding author. Department of Physics, Faculty of Science, University of M'sila, 28000, M'sila, Algeria.
E-mail addresses: baaziz_hakim@yahoo.fr, hakim.baaziz@univ-msila.dz (H. Baaziz).

https://doi.org/10.1016/j.mssp.2024.109185
Received 7 September 2024; Received in revised form 25 November 2024; Accepted 28 November 2024

first-principles calculations have been employed to probe the elastic, electronic, and optical properties of these compounds, with $ZnGeAs_2$ studied by Aditi et al. [11], and $CdSiAs_2$ and $ZnSiAs_2$ investigated by Boukabrine et al. [12]. In addition, the elastic and electronic properties of $ZnSnP_2$ have been analyzed by Sahin et al. [13], shedding light on their potential as multifunctional materials.

Despite these advancements, much of the existing research remains fragmented, with most studies focusing on isolated properties without providing a holistic understanding of the interconnections between structure, electronic band structure, optical response, and thermoelectric performance. Moreover, temperature-dependent thermoelectric behavior, which is crucial for optimizing materials for energy harvesting, has not been extensively explored for these compounds.

The development of portable electronics, energy-efficient devices, and renewable energy systems has further driven the demand for materials with tunable and enhanced physical properties. Researchers have been actively working on methods to modify and improve the performance of chalcopyrite materials, often by doping or partial substitution of elements. For instance, Fedorchenko et al. [14] studied the structural and magnetic properties of II-IV-V_2 semiconductors doped with Mn, while Anna et al. [15] investigated the magnetic properties of A^{II}-B^{IV}-C^{V}_2 chalcopyrite semiconductors doped with 3d-elements, identifying them as potential candidates for spintronics. Similarly, Mouacher et al. [16] explored the structural, electronic, and optical properties of $AgGaS_2$, demonstrating that $AgGa_{1-x}Tl_xS_2$ alloys hold significant promise for optoelectronic and photovoltaic applications.

Building on these advancements, $ZnGeAs_2$ and $ZnSiAs_2$ have emerged as leading candidates for a variety of energy-related applications due to their direct band gaps, favorable optical properties, and potential for high thermoelectric efficiency. However, several critical issues remain unresolved. While some structural parameters, such as lattice constants and bond lengths, have been experimentally determined, their influence on the electronic band structure, density of states, and optical response requires deeper theoretical exploration. Most existing studies focus narrowly on individual properties, such as elasticity or optical behavior, without examining the interconnections between structural, electronic, optical, and thermoelectric properties. Furthermore, a detailed understanding of the temperature-dependent thermoelectric behavior of $ZnGeAs_2$ and $ZnSiAs_2$, including key parameters like the Seebeck coefficient, electrical conductivity, and lattice thermal conductivity, is essential for optimizing their performance in photovoltaic, optoelectronic, and energy harvesting devices.

This study aims to address these gaps by employing first-principles density functional theory (DFT) calculations to systematically investigate the structural, electronic, optical, and thermoelectric properties of $ZnGeAs_2$ and $ZnSiAs_2$. Specifically, this work seeks to elucidate the relationship between structural parameters (e.g., lattice constants, bond lengths) and the electronic and optical behavior of these materials. Additionally, we provide a comprehensive analysis of their temperature-dependent thermoelectric properties, including the Seebeck coefficient, electrical conductivity, and figure of merit (ZT), to assess their suitability for energy applications. By bridging the gap between experimental observations and theoretical predictions, this work aims to guide the future design of chalcopyrite-based materials for optoelectronic and thermoelectric applications.

This paper is organized as follows: Section 2 describes the computational methodology employed in this work, detailing the DFT framework and relevant approximations. Section 3 presents and discusses the most relevant results for the structural, electronic, optical, and thermoelectric properties of $ZnGeAs_2$ and $ZnSiAs_2$. Finally, Section 4 provides conclusive remarks, summarizing the findings and outlining potential directions for future research.

2. Computational details

In this work, we investigate the structural, electronic, optical, and thermoelectric properties of the ternary chalcopyrite pnictide semiconductors $ZnGeAs_2$ and $ZnSiAs_2$, which crystallize in a tetragonal structure with the space group $I\bar{4}2d$ [3]. We also study their related quaternary alloys $ZnGe_{1-x}Si_xAs_2$, aiming to understand how partial substitution of Ge with Si affects the material properties. Our study employs the first-principles full potential linearized augmented plane wave (FP-LAPW) method as implemented in the WIEN2k code [17,18]. The local density approximation (LDA) [19] and the generalized gradient approximation (GGA) [20] were applied for a thorough treatment of the exchange and correlation energy functional in the calculations of structural properties.

The electronic structure of chalcopyrite alloys is particularly important for their applications in optoelectronics and thermoelectrics. However, the GGA approach often underestimates band gap values, which can lead to inaccurate predictions of electronic properties. To address this, we examined the electronic structure using the modified Becke-Johnson (mBJ) potential [21], which provides more accurate band gap predictions.

Optical properties, such as dielectric function, refractive index, and absorption coefficient, are essential for applications in photovoltaics and optoelectronics. These properties are influenced by the electronic structure and can exhibit anisotropic behavior depending on the crystallographic direction. Our study investigates these optical properties to understand how they vary with composition and structural changes.

Thermoelectric properties are another critical aspect, particularly for energy conversion applications. Materials with high Seebeck coefficients, low thermal conductivity, and high electrical conductivity are desirable for thermoelectric applications. We computed the thermoelectric characteristics of the investigated alloys using the BoltzTraP code [22], focusing on parameters such as the Seebeck coefficient, electrical conductivity, and thermal conductivity.

The all-electron FP-LAPW approach, implemented in the computational package WIEN2k [17,18], was utilized for the calculations of the $ZnGe_{1-x}SixAs_2$ alloys (x = 0, 0.25, 0.5, 0.75, and 1). This method uses density functional theory (DFT) in combination with the Kohn-Sham (KS) equations [23,24] to calculate the energy of the ground state and the electronic structure. For structural properties, the local density approximation and the revised Perdew-Burke-Ernzerhof (PBE) [19,20] were applied to calculate exchange-correlation energy. The modified Becke-Johnson (mBJ) potential [21] was also used to improve the precision of electronic and optical properties, as LDA and GGA are known to underestimate band gaps. For total energy calculations, we employed 1000 k-points in the first Brillouin zone. Additionally, we set $RMT \times k_{Max} = 8$ and used muffin-tin radii of 1.99, 2.11, 1.95, and 1.89 a.u. for Zn, Ge, Si, and As atoms, respectively. The energy convergence criterion was set to 10^{-4} Ry.

The thermoelectric properties of $ZnGe_{1-x}Si_xAs_2$ alloys, specifically thermal conductivity ($\kappa_e = k_0 - T\sigma S^2$), Seebeck coefficient (S), and electrical conductivity (σ), are calculated using Boltzmann transport theory under the constant relaxation time approximation, as described by the following equations [25,26]:

$$\sigma = e^2 \sum_k \left(-\frac{\partial f_0}{\partial \varepsilon} \right) \tau_{\vec{k}} v_{\vec{k}} v_{\vec{k}} \quad (1)$$

$$S = e k_B \sigma^{-1} \sum_k \left(-\frac{\partial f_0}{\partial \varepsilon} \right) \tau_{\vec{k}} v_{\vec{k}} v_{\vec{k}} \frac{\varepsilon_k - \mu}{k_B T} \quad (2)$$

$$k_0 = k_B^2 T \sum_k \left(-\frac{\partial f_0}{\partial \varepsilon} \right) \tau_{\vec{k}} v_{\vec{k}} v_{\vec{k}} \left[\frac{\varepsilon_k - \mu}{k_B T} \right]^2 \quad (3)$$

3. Results and discussion

3.1. Structural parameters

The equilibrium structural parameters of the ternary II-IV-V_2 semiconductor family, specifically $ZnGeAs_2$, $ZnSiAs_2$, and their mixed quaternary alloys $ZnGe_{1-x}Si_xAs_2$ with varying concentrations (x = 0.25, 0.5, and 0.75), were examined in this study. These compounds crystallize in the tetragonal chalcopyrite structure, characterized by the space group $I\bar{4}2d$ as illustrated in Fig. 1. The parameters analyzed include the lattice constants (a and c), the bulk modulus (B), and its pressure derivative (B′). These parameters were determined by fitting the total energy-volume data to Murnaghan's equation of state (M-EOS) [27].

Accurate determination of the structural parameters is crucial, as they significantly influence the electronic, optical, and thermoelectric properties of the materials. The lattice constants, *a* and *c*, define the dimensions of the unit cell, while the bulk modulus, B, provides an indication of the material's resistance to volume changes under pressure. The pressure derivative of the bulk modulus, B′, offers insights into the compressibility of the material. Additionally, internal cell parameters, such as the positional parameter u, are vital for understanding the atomic arrangement within the unit cell [28].

For the $ZnGe_{1-x}Si_xAs_2$ alloys (x = 0, 0.25, 0.5, 0.75, and 1), the obtained results for the lattice parameters *a* and *c* (in Å), bulk modulus B (in GPa), and internal cell parameter u are shown in Table 1. These results are compared with available experimental data and other theoretical results. We observed that the LDA approximation tends to underestimate the structural parameters, whereas the GGA values show reasonable agreement with experimental data [8–10,29,30] and previous theoretical results [12,31] for $ZnGeAs_2$ and $ZnSiAs_2$.

Our findings reveal that the geometrical parameter η, defined as c/2a, deviates from unity (η = 1), indicating a distortion effect caused by interactions between second-neighbor atoms. This deviation is significant as it reflects the degree of tetragonal distortion in the chalcopyrite structure. Such distortions can have a profound impact on the electronic band structure and, consequently, on the material's optical and thermoelectric properties.

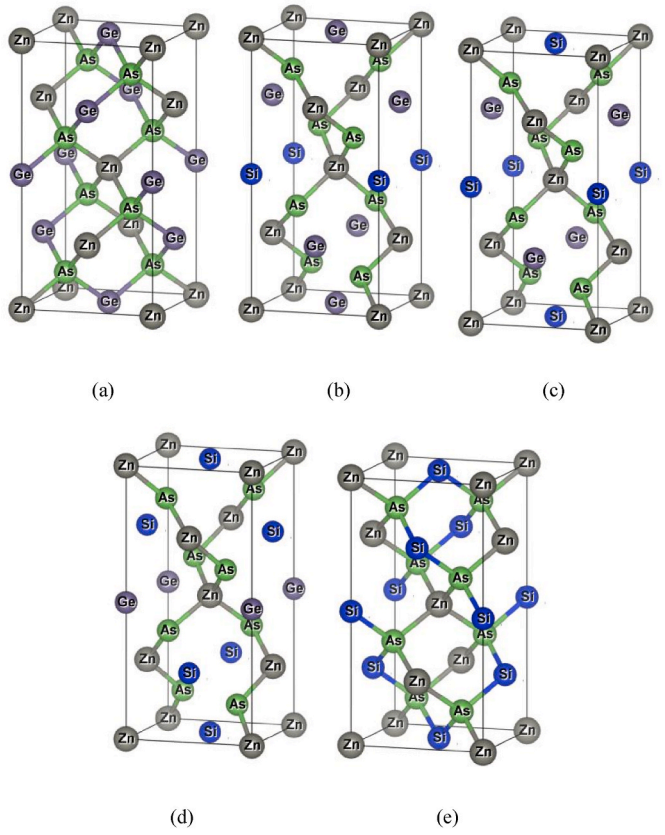

Fig. 1. Crystal structure of the $ZnGe_{1-x}Si_xAs_2$ chalcopyrite alloys (a) $ZnGeAs_2$ (b) $ZnGe_{0.75}Si_{0.25}As_2$ (c) $ZnGe_{0.5}Si_{0.5}As_2$ (d) $ZnGe_{0.25}Si_{0.75}As_2$ (e) $ZnSiAs_2$.

Table 1
The calculated lattice constants (a and c), bulk modulus and its derivative, internal parameters (η and u) for $ZnGe_{1-x}Si_xAs_2$ alloys (x = 0, 0.25, 0.5, 0.75 and 1) using LDA and GGA approximations.

X	Parameters	LDA	GGA	Experimental	Others
0	a (Å)	5.615	5.670	5.672 [9]	5.663 [31]
	c (Å)	11.089	11.192	11.153 [9], 11.192 [8]	11.22 [31]
	c/a	1.975	1.974	1.966 [9]	1.981 [31]
	Δa/a (%)	−1.005	−0.035		
	Δc/c (%)	−0.574	0.349		
	B (GPa)	74.40	69.24	67 [29]	67 [31]
	B'	4.62	4.66		4.97 [31]
	u	0.256	0.256		0.254 [31]
	η	0.987	0.987	0.9824 [30]	
0.25	a (Å)	5.634	5.689		
	c (Å)	11.663	11.671		
	c/a	2.070	2.051		
	B (GPa)	73.72	68.18		
	B'	4.51	4.52		
	u	0.233	0.237		
	η	1.035	1.026		
0.5	a (Å)	5.627	5.679		
	c (Å)	11.642	11.763		
	c/a	2.069	2.071		
	B (GPa)	74.58	69.55		
	B'	4.58	4.69		
	u	0.233	0.232		
	η	1.034	1.036		
0.75	a (Å)	5.625	5.674		
	c (Å)	11.735	11.856		
	c/a	2.086	2.089		
	B (GPa)	75.366	70.39		
	B'	4.65	4.70		
	u	0.229	0.228		
	η	1.043	1.045		
1	a (Å)	5.555	5.604	5.612 [10]	5.5591 [12], 5.584 [31]
	c (Å)	10.848	10.945	10.878 [10]	10.862 [12], 10.95 [31]
	c/a	1.958	1.953	1.938 [10]	1.9540 [12], 1.960 [31]
	Δa/a (%)	−1.016	−0.142		
	Δc/c (%)	−0.27	0.615		
	B (GPa)	81.00	76.22	68 [29]	81.49 [12], 76 [31]
	B'	4.56	4.59		4.46 [12], 4.66 [31]
	u	0.262	0.262		0.259 [31]
	η	0.976	0.976	0.9698 [30]	

In the case of the quaternary alloys $ZnGe_{1-x}Si_xAs_2$, where x = 0.25, 0.5, and 0.75, no experimental or theoretical data are available for comparison. Therefore, our calculated values provide a valuable reference for these compositions. These results may serve as a benchmark for future experimental and theoretical studies, aiding in the synthesis and characterization of these alloys.

To summarize, the structural parameters determined in this study underscore the importance of accurate theoretical calculations in predicting material properties. The reasonable agreement between our GGA results and experimental data for $ZnGeAs_2$ and $ZnSiAs_2$ confirms the reliability of our computational approach. Moreover, the predicted structural parameters for the quaternary alloys $ZnGe_{1-x}Si_xAs_2$ broaden the understanding of these materials and provide new insights into their potential applications.

Our calculations show that the lattice constants of the $ZnGe_{1-x}Si_xAs_2$

alloys decrease with increasing Si content (x). This reduction is attributed to the smaller atomic radius of Si compared to Ge. For example, $ZnGeAs_2$ has a larger lattice constant than $ZnSiAs_2$, and the intermediate alloys exhibit a linear reduction following Vegard's law, indicating that the alloys form stable solid solutions. The substitution of Ge with Si reduces the bond lengths between the cations (Zn, Si) and the anions (As), leading to stronger bonds in the alloys with higher Si content. This increased bond strength enhances the structural stability of the alloys.

This stability increases with Si content due to the stronger Zn–Si and Si–As bonds, which are less polarizable than Zn–Ge and Ge–As bonds. This trend aligns with observations in similar alloy systems, such as $GaAs_{1-x}P_x$ or $InAs_{1-x}P_x$.

3.2. Electronic properties

In this study, we examine the electronic properties of the ternary compounds $ZnGeAs_2$, $ZnSiAs_2$, and their mixed quaternary alloys $ZnGe_{1-x}Si_xAs_2$ with varying concentrations of Si (x = 0.25, 0.5, and 0.75) using both the generalized gradient approximation (GGA) and the modified Becke-Johnson (mBJ-GGA) approach. The electronic band structures for $ZnGe_{1-x}Si_xAs_2$ alloys along the high-symmetry directions of the first Brillouin zone are shown in Fig. 2. For convenience, the Fermi energy is set at 0 eV, and the computed band gap values using both approximations are listed in Table 2.

The electronic band structures of the alloys under consideration display a consistent overall structure, indicating that the fundamental electronic characteristics remain unchanged when the Ge atom is substituted with Si. However, significant differences are observed in the band gap values, as shown in Table 2. Specifically, the mBJ-GGA approximation yields larger band gap values compared to GGA. Both the minimum of the conduction band and the maximum of the valence band occur at the high-symmetry point Γ of the first Brillouin zone, confirming that the $ZnGe_{1-x}Si_xAs_2$ alloys are semiconductors with a direct band gap at the Γ point.

The direct band gap nature of these alloys is crucial for optoelectronic applications, particularly for infrared detectors, as suggested by Ref. [6]. The band gap values for the mixed alloys (x = 0.25, 0.5, and 0.75) are observed to decrease compared to the parent compounds $ZnGeAs_2$ and $ZnSiAs_2$. This trend is significant because it indicates the tunability of the electronic properties through compositional variation, which is beneficial for designing materials with specific optical and electronic characteristics.

Table 2
The calculated band gap values within GGA and mBJ- GGA approximations.

X	Eg			
	Our work		Experimental	Others
	GGA	mBJ-GGA		
0	0.567	1.354	1.15 [8], 1.37 [32], 1.2 [33], 1.1 [34],	0.13 [2], 0.536 [35], 1.16 [36], 1.2 [31,37], 1.27 [38]
0.25	0.112	0.717		
0.5	0.052	0.623		
0.75	0.077	0.632		
1	1.163	1.878	2.12 [1], (1.76–2.16) [39], 2.1 [40]	0.91 [2], 1.007 [12], 1.7 [31]

Table 2 provides a detailed comparison of the band gap values for $ZnGeAs_2$ and $ZnSiAs_2$ using both GGA and mBJ-GGA approximations. It is clear that the mBJ-GGA approximation yields band gap values that are in better agreement with experimental results. This observation aligns with the well-established understanding that mBJ improves the accuracy of band gap calculations over GGA, making it a preferred choice for electronic structure investigations.

The accurate determination of band gap values is essential for predicting the performance of semiconductors in various applications. The direct band gap at the Γ point in $ZnGe_{1-x}Si_xAs_2$ alloys suggests their potential effectiveness in light-emitting devices and photovoltaic cells, where efficient electron-hole recombination is desired. Additionally, the ability to tailor the band gap through compositional adjustments offers a pathway for optimizing these materials for specific technological applications.

To summarize, our study demonstrates that the $ZnGe_{1-x}Si_xAs_2$ alloys display direct band gaps at the Γ point, with band gap values decreasing as the Si concentration increases. The use of the mBJ-GGA approximation yields more accurate band gap predictions compared to GGA, emphasizing the significance of selecting appropriate computational methods for electronic structure analysis. These findings enhance the

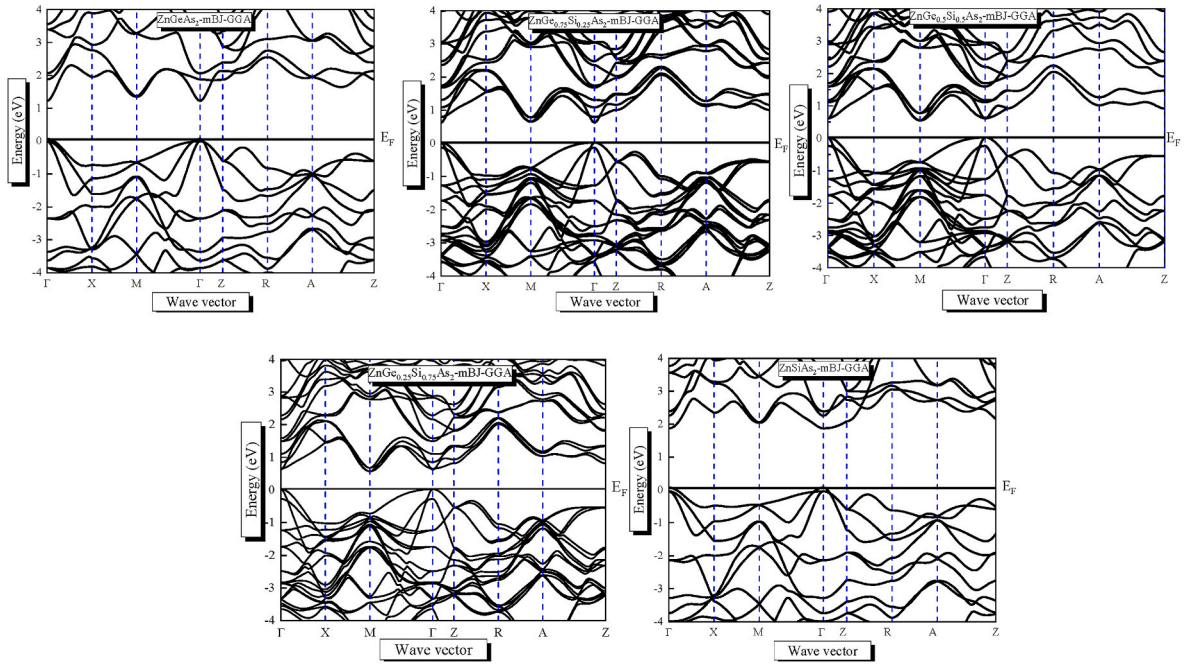

Fig. 2. The band structure of $ZnGe_{1-x}Si_xAs_2$ (x = 0, 0.25, 0.5, 0.75 and 1) chalcopyrite alloys using mBJ-GGA approximation.

understanding of the electronic properties of chalcopyrite semiconductors and their potential applications in optoelectronics and infrared detection.

The density of states (DOS) provides valuable insight into the distribution of available electronic states at each energy level within a material. In this study, we calculated both the partial and total density of states (PDOS and TDOS) using the modified Becke-Johnson generalized gradient approximation (mBJ-GGA) for $ZnGe_{1-x}Si_xAs_2$ alloys with varying Si concentrations (x = 0, 0.25, 0.5, 0.75, and 1). The results are presented in Fig. 3, which illustrates the distribution of electronic states within these alloys. The TDOS curves in Fig. 3 reveal three distinct energy regions, which can be categorized as the lower valence band (LVB), upper valence band (UVB), and conduction band (CB).

(i) The LVB, spanning from −8.5 eV to −6.5 eV, is primarily composed of Zn-d states, with a noticeable mixture of Si/Ge s-p states and a minor contribution from As s-p states. The presence of Zn-d states reflects strong bonding interactions between Zn and the other constituent atoms, contributing significantly to the material's overall stability.

(ii) The UVB, ranging from −6.5 eV to 0 eV, is dominated by Si-Ge p states and As-p states, arising from the strong hybridization between Ge-p and As-p states. The substantial overlap of these p states indicates a robust covalent bonding character within the valence band, which is crucial for determining the electronic properties of the alloys.

(iii) The CB, extending from 0 eV to 6 eV, is characterized by the strong hybridization between Si/Ge s states and As-p states, with minor contributions from Si/Ge p and As-s states. The states near the Fermi level in the conduction band are critical for understanding the material's conductivity and electron mobility.

As the Si concentration increases, significant changes in the DOS are observed. Specifically, the peak corresponding to the Si p states becomes more prominent, while the peak associated with the Ge p states diminishes. This shift indicates that the electronic structure is substantially influenced by the substitution of Ge atoms with Si atoms, leading to changes in the bonding environment and the overall electronic properties.

The PDOS analysis provides valuable insight into the contributions of individual atomic states to the overall electronic structure. The

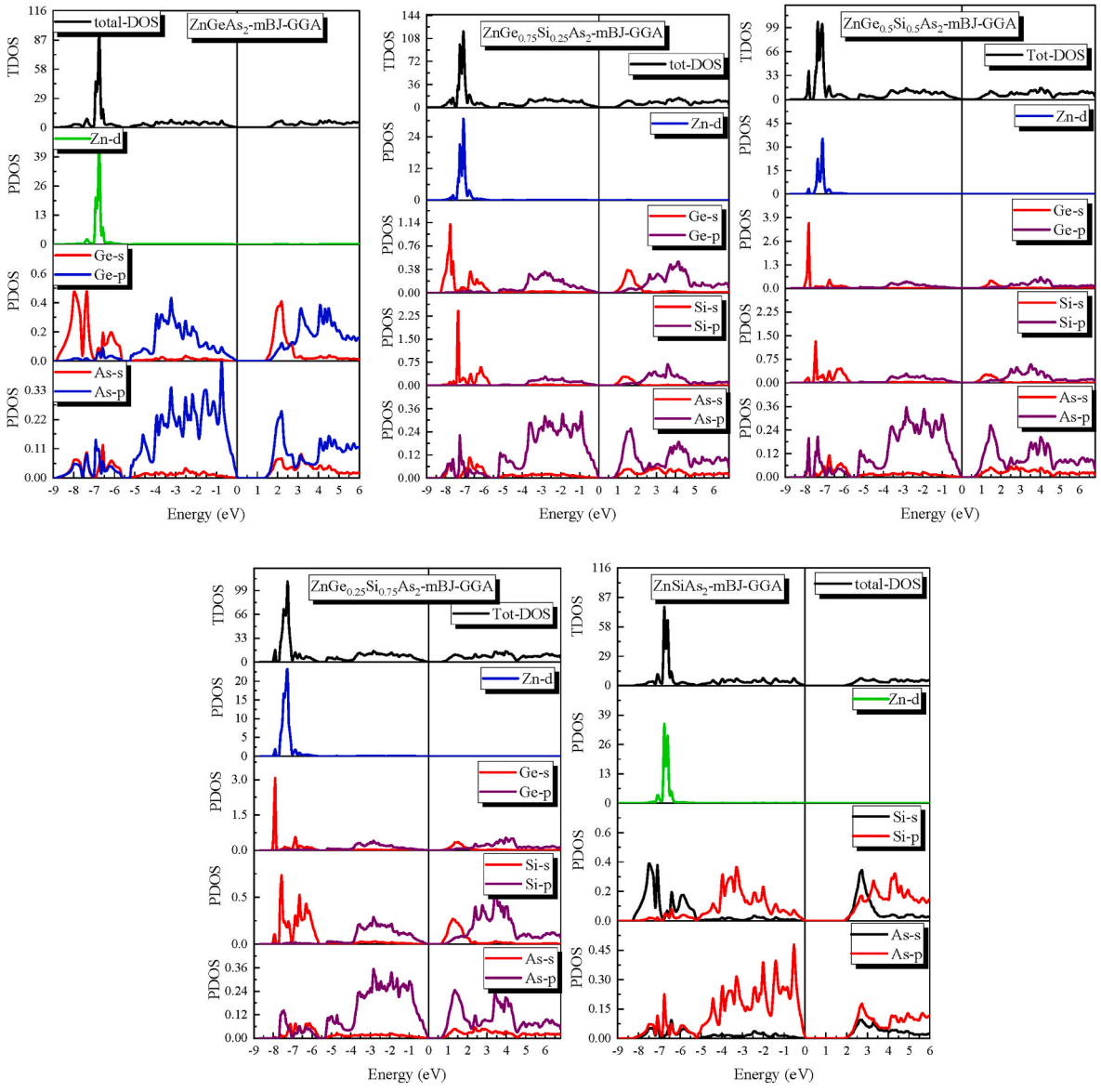

Fig. 3. The calculated density of states of $ZnGe_{1-x}Si_xAs_2$ (x = 0, 0.25, 0.5, 0.75 and 1) chalcopyrite alloys using mBJ-GGA approximation.

introduction of Si atoms leads to the formation of additional p states, which become more intense with higher Si concentrations. In contrast, the intensity of the Ge p states decreases, reflecting the reduction in Ge content. This substitution effect emphasizes the tunability of the electronic properties by varying the alloy composition, making these materials highly versatile for a wide range of applications.

The detailed DOS analysis further enhances our understanding of the electronic behavior of $ZnGe_{1-x}Si_xAs_2$ alloys. The ability to tailor the electronic structure through compositional adjustments provides key insights for optimizing these materials for specific technological applications, such as infrared detectors and other optoelectronic devices. The insights gained from the DOS calculations complement and reinforce the band structure analysis, offering a holistic view of the electronic properties of these chalcopyrite semiconductors.

The band gap of $ZnGe_{1-x}Si_xAs_2$ increases with Si substitution, following the trend between the two parent compounds ($ZnGeAs_2$ with a smaller gap and $ZnSiAs_2$ with a larger gap). This is due to the stronger covalent bonding and reduced lattice constant in alloys with higher Si content. The direct band gap nature is preserved across all compositions, making the alloys suitable for optoelectronic applications. This behavior is characteristic of chalcopyrite alloys, as seen in other systems like $GaAs_{1-x}P_x$.

3.3. Optical properties

Understanding the optical properties of materials is essential for their application in optoelectronic devices, such as photodetectors, light-emitting diodes, and solar cells. The optical behavior of a material is fundamentally characterized by how it interacts with light, including absorption, reflection, refraction, and energy loss mechanisms. For the $ZnGe_{1-x}Si_xAs_2$ alloys, analyzing these properties offers valuable insight into their potential utility in various optical and electronic applications.

In this section, we examine the optical characteristics of $ZnGe_{1-x}Si_xAs_2$ alloys by employing first-principles calculations. We focus on the complex dielectric function $\varepsilon(\omega) = \varepsilon_1(\omega) + i\varepsilon_2(\omega)$, which is a key parameter for understanding the material's response to electromagnetic radiation. This function allows us to derive several important optical properties, including the extinction coefficient, refractive index, optical conductivity, absorption coefficient, reflectivity, and energy loss spectrum. The complex dielectric function is divided into two components:

The imaginary component of the dielectric function that depends on frequency $\varepsilon_2(\omega)$ given by the following relation:

$$\varepsilon_2(\omega) = \frac{4\pi^2 e^2}{m^2\omega^2}\sum\int \langle i|M|j\rangle^2 f_i(1-f_i)\sigma\left[E_f - E_i - \omega\right]d^3k \tag{4}$$

- The real component of dielectric $\varepsilon_1(\omega)$ which is obtained from the matrix of the imaginary part of dielectric $\varepsilon_2(\omega)$ by the applications of the Kramer's Kronig relation [41]:

$$\varepsilon_1(\omega) = 1 + P\left(\frac{2}{\pi}\right)\int_0^\infty \frac{\omega'\varepsilon_2(\omega')}{\omega'^2 - \omega^2}d\omega' \tag{5}$$

The other important optical properties including extinction coefficient $k(\omega)$, and refractive index $n(\omega)$, optical conductivity $\sigma(\omega)$, absorption coefficient $I(\omega)$, reflectivity $R(\omega)$ and the energy loss spectrum $L(\omega)$ are computed using the given relations [42,43]:

$$k(\omega) = \sqrt{\frac{(\varepsilon_1(\omega)^2 + \varepsilon_2(\omega)^2)^{\frac{1}{2}} - \varepsilon_1(\omega)}{2}} \tag{6}$$

$$n(\omega) = \sqrt{\frac{(\varepsilon_1(\omega)^2 + \varepsilon_2(\omega)^2)^{\frac{1}{2}} + \varepsilon_1(\omega)}{2}} \tag{7}$$

$$\sigma(\omega) = \frac{\omega}{4\pi}\varepsilon_2(\omega) \tag{8}$$

$$I(\omega) = \frac{4\pi}{\lambda}k(\omega) \tag{9}$$

$$R(\omega) = \frac{(n(\omega)-1)^2 + k(\omega)^2}{(n(\omega)+1)^2 + k(\omega)^2} \tag{10}$$

$$L(\omega) = \frac{\varepsilon_2(\omega)}{\varepsilon_1^2(\omega) + \varepsilon_2^2(\omega)} \tag{11}$$

In Fig. 4(a–d), we present our calculated real and imaginary parts of the dielectric function $\varepsilon(\omega)$, extinction coefficient $k(\omega)$, and refractive index $n(\omega)$, using the mBJ-GGA exchange-correlation (xc) functional for the $ZnGe_{1-x}Si_xAs_2$ alloys, covering photon energy up to 14 eV. The estimated optical parameters at the zero-frequency limit, such as $\varepsilon_1(0)$, $\varepsilon_2(0)$, n(0), R(0), L(0), and the uniaxial anisotropy ($\delta\varepsilon$) of the investigated alloys using both GGA and mBJ-GGA xc functionals, are extracted and listed in Table 3.

It can be seen from Table 3 that our calculated values of optical parameters at the zero-frequency limit are in good agreement with previous theoretical data [11,12,31,35] for the parent $ZnGeAs_2$ and $ZnSiAs_2$. Furthermore, there is a clear difference between the perpendicular and parallel components of the real and imaginary parts of the

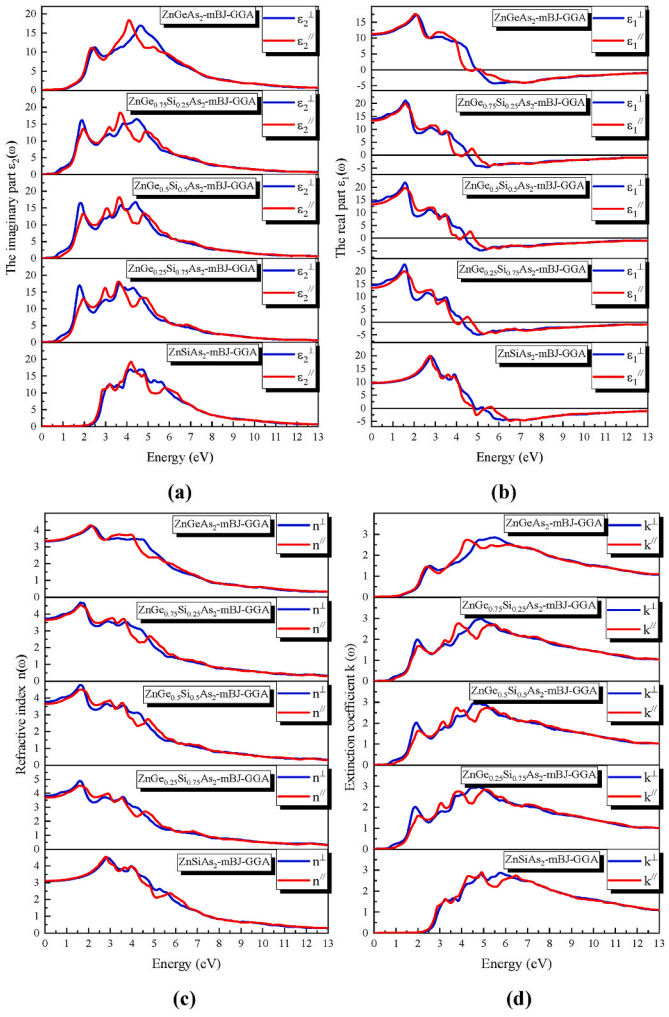

Fig. 4. Plot of dielectric function (real and imaginary part), refractive index $n(\omega)$ and extinction coefficient $k(\omega)$ for $ZnGe_{1-x}Si_xAs_2$ at (x = 0, 0.25, 0.5, 0.75 and 1) using mBJ-GGA.

Table 3
The calculated values of $\varepsilon_1(0)$, $n(0)$, $R(0)$ and $L(0)$ and the uniaxial anisotropy ($\delta\varepsilon$) for $ZnGe_{1-x}Si_xAs_2$ alloys (x = 0, 0.25, 0.5, 0.75 and 1) within GGA, mBJ-GGA.

X	$\varepsilon_1(0)$			$n(0)$		$R(0)$		$L(0).\ 10^{-4}$		Ref
	$\varepsilon_1^{\perp}$	$\varepsilon_1^{//}$	$\delta\varepsilon$	$n^{\perp}$	$n^{//}$	$R^{\perp}$	$R^{//}$	$L^{\perp}$	$L^{//}$	
0	17.306	17.880	0.016	4.160	4.228	0.375	0.381	6.958	7.123	GGA
	11.069	11.292	0.001	3.327	3.361	0.289	0.293	11.4	11.5	mBJ-GGA
		10.88			3.32					[11]
				3.32						[31]
	16.37			4.04						[35]
0.25	24.989	22.303	−0.057	4.999	4.723	0.444	0.423	11.7	7.871	GGA
	13.959	13.347	−0.022	3.736	3.653	0.334	0.325	6.366	6.171	mBJ-GGA
0.5	19.049	16.403	−0.074	4.365	4.050	0.393	0.365	13.5	10.5	GGA
	14.275	13.345	−0.034	3.778	3.653	0.338	0.325	6.422	6.104	mBJ-GGA
0.75	22.308	17.903	−0.109	4.724	4.231	0.423	0.381	20	9.333	GGA
	14.521	13.546	−0.035	3.811	3.681	0.341	0.328	6.349	6.029	mBJ-GGA
1	13.322	13.612	0.011	3.650	3.689	0.325	0.329	5.089	5.177	GGA
	9.546	9.669	0.006	3.090	3.109	0.261	0.263	5.335	5.391	mBJ-GGA
	6.5095	6.8104		3.6082	3.6906					[12]
				3.12						[31]

dielectric function, indicating that these materials exhibit uniaxial anisotropy. This is also confirmed by the calculated uniaxial anisotropy from the following relation [44]:

$$\delta\varepsilon = \frac{\varepsilon_{1zz}(0) - \varepsilon_{1xx}(0)}{\varepsilon_{tot}(0)} \tag{12}$$

We note also that the static dielectric constant is higher for composition x = 0.75 and lowest for x = 1.

According to Fig. 4a, ($\varepsilon_1\hat{}\perp/\varepsilon_1\hat{}(//)$) spectra increase with energy for all the alloys examined and reach maximum values of (17.2863/17.6148), (21.1295/19.9744), (21.7897/19.7463), (22.7085/20.031), and (19.8599/19.9133) around 2.1 eV, 1.59 eV, 1.56 eV, 1.54 eV, and 2.77 eV for $0 \le x \le 1$ with a step of 0.25. After that, the curves show a downhill trend after these peaks, turn negative, and approach a minimum value. The negative values indicate the metallic property, which occurs when all incoming electromagnetic radiation is reflected off the material's surface [45]. It is found that the main peaks of $\varepsilon_1(\omega)$ spectra move towards lower energies for $x < 0.75$, then shift toward higher energies for $x > 0.75$.

As shown in Fig. 4b, the main peaks of ($\varepsilon_2\hat{}\perp/\varepsilon_2\hat{}(//)$) spectrum are located at around (4.63 eV/4.09 eV), (4.47 eV/3.71 eV), (4.42 eV/3.63 eV), (3.66 eV/3.60 eV), and (4.64 eV/4.09 eV) for Si concentrations (x = 0.00, 0.25, 0.5, 0.75, and 1.00), respectively. Furthermore, we observed that these peaks move towards lower energies with increasing Si concentration for ($0 < x < 0.75$), while they move towards higher energies for the remainder of concentrations. It can be observed that there is strong absorption in the energy range (1.5–6.5) eV.

According to Table 4, the static values of $\varepsilon_1(0)$ and n(0) are consistent with the formula $\varepsilon_1(0) = n(0)^2$. Therefore, static values of the refractive index $n(0)$ vary similarly to those of $\varepsilon_1(0)$. From Fig. 4c, the refractive index's ordinary $n\hat{}\perp$ and extraordinary $n\hat{}(//)$ components show anisotropic behavior between the two components. In the energy range of (0–6) eV, the anisotropy is clearly observable. Moreover, the maximum value of n(ω) occurs around (2.16 ± 0.06 eV) for $ZnGeAs_2$, (1.62 ± 0.03 eV) for $ZnGe_{0.75}Si_{0.25}As_2$, $ZnGe_{0.5}Si_{0.5}As_2$, $ZnGe_{0.25}Si_{0.75}As_2$, and (2.79 ± 0.05 eV) for $ZnSiAs_2$. The transparency of the material decreases as the refractive index value decreases. Thus, $ZnGe_{0.25}Si_{0.75}As_2$ has the highest refraction among these alloys with maximum transparency.

Table 4
Room temperature thermoelectric transport properties of $ZnGe_{1-x}Si_xAs_2$ at (x = 0, 0.25, 0.5, 0.75 and 1) using mBJ-GGA.

	n (10^{18} cm^{-3})	$(\sigma/\tau)10^{18}$ (Ω m s)$^{-1}$	$(K_e/\tau)10^{14}$W(m. k.s)$^{-1}$	S(μV/K)
$ZnGeAs_2$	67.9	4.63	0.69	166
$ZnGe_{0.75}Si_{0.25}As_2$	32.6	2.64	0.44	188
$ZnGe_{0.5}Si_{0.5}As_2$	32.8	2.85	0.44	179
$ZnGe_{0.25}Si_{0.75}As_2$	31.5	2.69	0.44	186
$ZnSiAs_2$	83.7	4.72	0.72	165

The extinction coefficient k(ω) indicates the material's light-absorbing abilities, similar to $\varepsilon_2(\omega)$. It is noticed from Fig. (4d) that the maximum of k(ω) for our alloys at (x = 0, 0.25, 0.5, 0.75, and 1) respectively occurs in photon energy at 5.48(4.23) eV, 4.86(3.88) eV, 4.53(3.77) eV, 4.77(5.07) eV, and 5.75(4.91) eV for K^⊥(K^(//)).

Fig. (5a–d) illustrates the spectra of optical conductivity σ(ω), absorption coefficient I(ω), reflectivity R(ω), and the energy loss spectrum L(ω) for our investigated alloys under the mBJ-GGA approximation.

It is clearly seen, from Fig. 5a, that the optical conductivity σ(ω) for $ZnGe_{1-x}Si_xAs_2$ at (x = 0, 0.25, 0.5, 0.75, and 1) respectively rises and reaches a maximum at 4.12 eV (4.69 eV), 3.71 eV (4.53 eV), 3.66 eV (4.42 eV), 3.63 eV (4.31 eV), and 4.20 eV (4.75 eV). In addition, the maximum optical conductivity at 4.69 eV (4.75 eV) for the parent $ZnGeAs_2$ and $ZnSiAs_2$, while $ZnGe_{0.25}Si_{0.75}As_2$ has the minimum at 4.31 eV for the perpendicular component σ^⊥.

According to Fig. 5b, the absorption of photons for our alloys starts at around (0.9 eV–2 eV) for $ZnGeAs_2$, $ZnSiAs_2$, respectively, and (0.8 eV) for (x = 0.25, 0.5, 0.75). The highest peaks in the absorption spectrum are observed at 7.33 eV, 7.66 eV, 7.6 eV, 7.47 eV, and 7.19 eV for I^(⊥), while the parallel component I^(//) shows a maximum at 7.17 eV, 7.41 eV, 7.36 eV, 7.25 eV, and 6.43 eV for $0 \le x \le 1$ with a step of 0.25. Compared to $ZnGe_{1-x}Si_xAs_2$ (x = 0.25, 0.5, 0.75), the parent $ZnGeAs_2$ and $ZnSiAs_2$ have a higher absorption coefficient. Furthermore, our results agree reasonably well with the experimental data from Ref. [8].

As is clear from Fig. 5c, for the alloys under consideration, the static part of these alloys' reflectivity R(ω) spectra starts at zero frequency, with values found to be equal to 28.9 %, 33.4 %, 33.8 %, 34.1 %, and 26.1 % for R^⊥, and 29.3 %, 32.5 %, 32.5 %, 32.8 %, and 26.3 % for R^(//) for the compositions (x = 0, 0.25, 0.5, 0.75, and 1), respectively. Also, R(0) for $ZnGeAs_2$ is in good agreement with the reported value of 28.6 % from Ref. [11].

The plots of the energy loss function L(ω) against photon energy for x ($0 \le x \le 1$) are displayed in Fig. 5d. It is observed that the maximum value of L(ω) is around 12.69 eV, 12.23 eV, 12.20 eV, 12.17 eV, and 12.91 eV for $ZnGeAs_2$, $ZnGe_{0.75}Si_{0.25}As_2$, $ZnGe_{0.5}Si_{0.5}As_2$, $ZnGe_{0.25}Si_{0.75}As_2$, and $ZnSiAs_2$, respectively. The $ZnGe_{0.25}Si_{0.75}As_2$ alloy loses more energy than the other alloys.

Si substitution shifts the absorption edge to higher energies due to the increased band gap, resulting in improved transparency in the visible

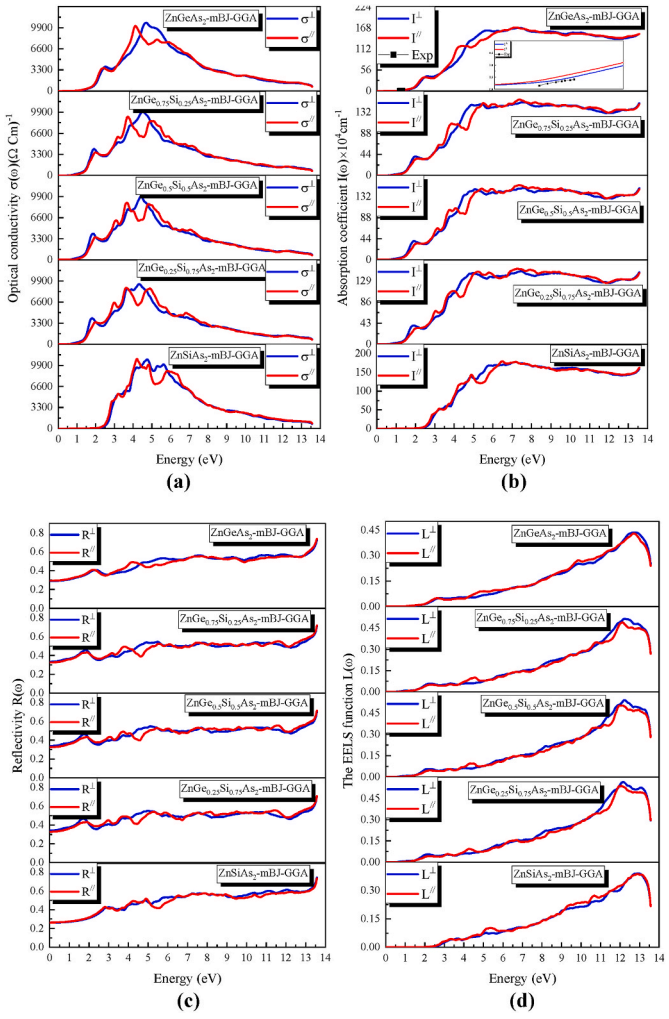

Fig. 5. Plot of the optical conductivity $\sigma(\omega)$, absorbance $I(\omega)$, reflectivity $R(\omega)$ and energy loss $L(\omega)$ for $ZnGe_{1-x}Si_xAs_2$ at (x = 0, 0.25, 0.5, 0.75 and 1) using mBJ-GGA.

range. The alloys exhibit high absorption coefficients and anisotropic behavior in the ultraviolet range. Among the alloys, $ZnGe_{0.25}Si_{0.75}As_2$ shows the highest refractive index and the most significant optical energy loss, while the high reflectivity in the ultraviolet region (>13.5 eV) suggests these materials are suitable for UV shielding.

3.4. Thermoelectric properties

In today's technology-driven world, managing heat loss and harnessing wasted thermal energy has become increasingly crucial. One promising approach is to convert excess heat into electrical energy using thermoelectric materials [46,47]. This study investigates the thermoelectric properties of chalcopyrite alloys $ZnGe_{1-x}Si_xAs_2$ (x = 0, 0.25, 0.5, 0.75, 1) using the BoltzTraP code, with a constant relaxation time approximation. The aim is to understand their potential for efficient thermoelectric energy conversion.

Fig. 6(a–f) illustrates the temperature-dependent behavior of key thermoelectric parameters, including electrical conductivity (σ), electronic thermal conductivity (K_e), lattice thermal conductivity (K_L), total thermal conductivity (K_T), Seebeck coefficient (S), and the figure of merit (ZT) across a temperature range from 50 K to 900 K. These parameters are crucial for evaluating the performance of thermoelectric materials.

Table 4 presents the thermoelectric transport properties at room temperature, offering detailed insights into the efficiency and suitability of these alloys for practical applications. The findings will help in assessing the potential of $ZnGe_{1-x}Si_xAs_2$ alloys for use in thermoelectric devices, contributing to advancements in energy conversion technologies.

3.4.1. Electrical conductivity (σ)

Figure (6a) shows the traces of the (σ/τ) in response to temperature change (T) for the $ZnGe_{1-x}Si_xAs_2$ alloys (x = 0, 0.25, 0.5, 0.75, 1). It is clear that as the temperature increases from T = 50 K to T = 900 K, electrical conductivity (σ/τ) also increases from (2.87, 1.50, 1.71, 1.51 and 3.01 to (13.49, 9.29, 8.78, 8.60 and 14.57) 10^{18} $(\Omega\ m\ s)^{-1}$ for $(0 \leq x \leq 1)$ with a step of 0.25. It can be seen that at room temperature $ZnSiAs_2$ has higher electrical conductivity as compared to $ZnGe_{1-x}Si_xAs_2$ for (x = 0, 0.25, 0.5, 0.75) this can be explained by its high carrier concentration as illustrated in Table 4.

3.4.2. Thermal conductivity K_T

In solids, total thermal conductivity (K_T) is caused by two mechanisms: heat transfer through lattice vibrations (K_L) and the movement of the charge carrier (K_e). These two contributions combine to regulate the overall transmission of thermal energy in the material, as indicated in the following equation [48]:

$$K_T = K_e + K_L \tag{13}$$

It is clear from figure (6b) that the electronic contribution to thermal conductivity over the relaxation time constant (K_e/τ) increases with temperature for all compositions range, which corresponds to the observed trend in electrical conductivity (σ/τ), this is due to the direct proportionality between σ and K_e, which is consistent with the Wiedemann-Franz law [49]. We can see from figure (6c) that the lattice thermal conductivity K_L of $ZnGe_{1-x}Si_xAs_2$ alloys at 300K are (3.53, 2.50, 2.42, 2.53)W/m.k and 4.36 for (x = 0, 0.25, 0.5, 0.75, 1) respectively. Furthermore, the lattice thermal conductivity decreases with increasing temperature from T = 50K to T = 900K, due of the increased ratio of phonon scattering caused by severe lattice vibration. Besides, various studies demonstrate that as temperature increases the lattice thermal conductivity decreases in accordance with this relationship $K_L \propto T^{-1}$ [50,51]. From figure (6d) the total thermal conductivity K_T of all our alloys decreases to reach minimum at T = 300 then it increases with increasing temperature. moreover, at room temperature the minimum thermal conductivity K_T^{min} is obtained for $ZnGe_{0.5}Si_{0.5}As_2$ alloy under the mBJ approach while the maximum value K_T^{max} obtained for $ZnSiAs_2$.

3.4.3. Seebeck coefficient (S)

The Seebeck coefficients were computed and plotted in figure (6e) for various temperatures to evaluate the thermoelectric performance of the $ZnGe_{1-x}Si_xAs_2$ alloys. As shown, $ZnGeAs_2$ is a p-type material because the Seebeck coefficient is positive, in agreement with previous experiments [9,34,52]. Notably, at 300 K, our alloy exhibits a maximum value of 188 μV/K for $ZnGe_{0.75}Si_{0.25}As_2$, while the minimum values are for $ZnGeAs_2$ and $ZnSiAs_2$ which are around 166 μV/K and 165 μV/K, respectively. At 800 K, the coefficient is 228 μV/K for $ZnGe_{0.75}Si_{0.25}As_2$.

3.4.4. Figure of merit ZT

The figure of merit ZT is a crucial factor to consider when assessing thermoelectric material efficiency. The ZT is equal to $(S^2\sigma)/K_T$. It considers the thermal conductivity (K_T), electrical conductivity (σ), and Seebeck coefficient (S). As shown, from the evolution of the figure of merit ZT with temperature for the $ZnGe_{1-x}Si_xAs_2$ alloys with (x = 0, 0.25, 0.5, 0.75, and 1.0) at the Fermi level in figure (6f), the ZT increases with temperature, reaching its maximum at T = 800 K. Notably, the highest values for ZT can be observed in $ZnGe_{0.75}Si_{0.25}As_2$.

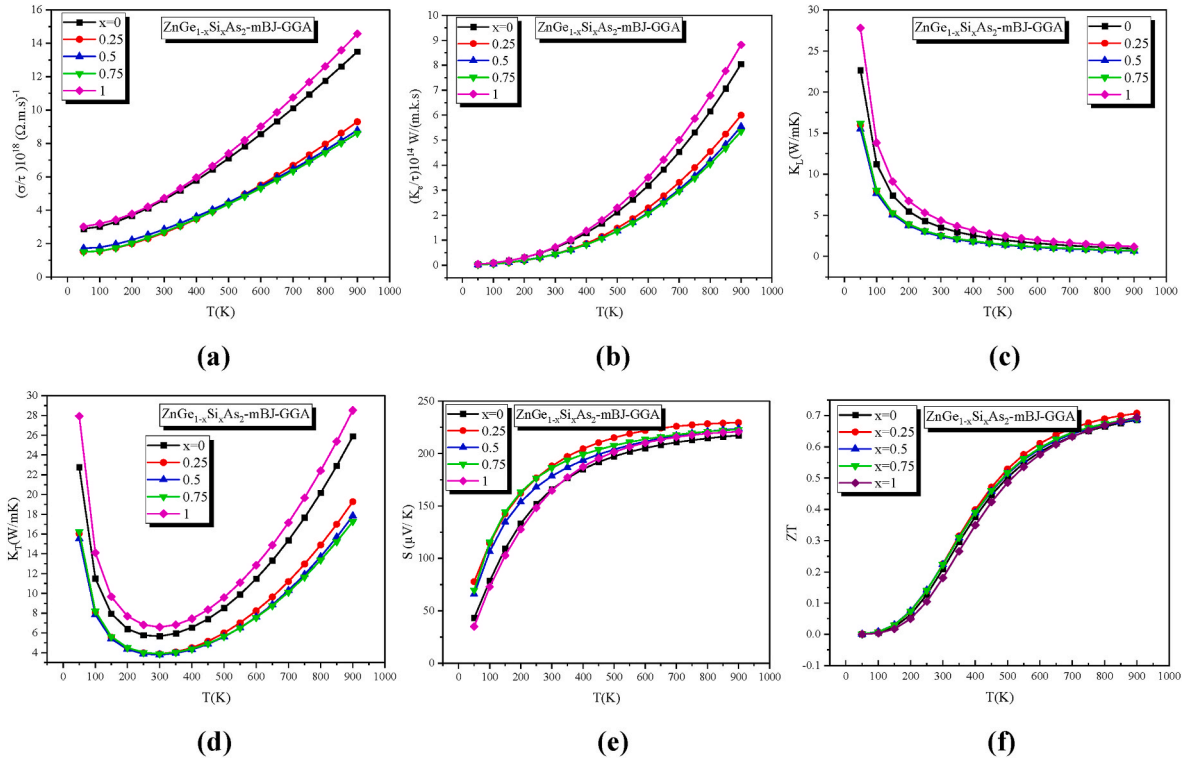

Fig. 6. Temperature dependency of the electrical conductivity (σ), electronic thermal conductivity (K_e), lattice thermal conductivity (K_L), total thermal conductivity (K_T), Seebeck coefficient (S) and Figure of merit (ZT) of $ZnGe_{1-x}Si_xAs_2$ at (x = 0, 0.25, 0.5, 0.75 and 1) using mBJ-GGA.

3.4.5. *The axial dependencies of thermoelectric properties for $ZnGe_{0.75}Si_{0.25}As_2$*

The $ZnGe_{0.75}Si_{0.25}As_2$ exhibits significant thermoelectric performance compared to the other alloys. We used the mBJ-GGA method to determine (S, (σ/τ), (K_e/τ)) in both directions (xx and zz). The electrical conductivity, Seebeck coefficients, and electronic component of the thermal conductivity tensors ($\sigma_{xx} = \sigma_{yy} \neq \sigma_{vv}$), ($S_{xx} = S_{yy} \neq S_{vv}$), ($K_{exx} = K_{eyy} \neq K_{evv}$) are diagonal.

As shown in Fig. 7(a and b), the electrical conductivity along the (xx) direction has larger values than the **(zz)** direction. This is due to a low density of states in the (zz) direction. Also, the electronic component of the thermal conductivity K_e/τ is almost the same in both directions for T < 300 K. With increasing temperature, the thermal conductivity K_{exx} becomes higher than K_{evv}.

As illustrated in Figure (7c), the $\mathbf{S}_{xx}$ Seebeck coefficient has higher values than the $\mathbf{S}_{vv}$ tensor in the temperature ranges of (50–100 K) and (800–900 K), but this trend is reversed in the temperature ranges (100–800 K), in which the $\mathbf{S}_{vv}$ tensor has larger values than the $\mathbf{S}_{xx}$ tensor. This indicates that the transport is dominated by the zz-axis for $100 \leq T \leq 800$ K.

Si substitution improves the thermoelectric performance of the alloys due to favorable changes in the Seebeck coefficient and electrical conductivity. $ZnGe_{0.75}Si_{0.25}As_2$ exhibits the best thermoelectric performance, with a Seebeck coefficient of 228.26 μV/K at 800 K, compared to $ZnGeAs_2$ and $ZnSiAs_2$. The anisotropic nature of the transport properties (e.g., $\sigma_{xx} \neq \sigma_{zz}$, $S_{xx} \neq S_{zz}$) allows for directionally optimized thermoelectric applications.

3.4.6. *Strategies for enhancing the Seebeck coefficient*

Fig. (8a) shows the variation of the Seebeck coefficient for $ZnGe_{0.75}Si_{0.25}As_2$ within a temperature range of 50–800 K. At 800 K, the value of S is 228.26 μV/K, which corresponds to a carrier concentration of $n = 119.74 \times 10^{18}$ cm^{-3}. To improve the thermoelectric performance of the $ZnGe_{0.75}Si_{0.25}As_2$ alloy, we investigated the impact of carrier

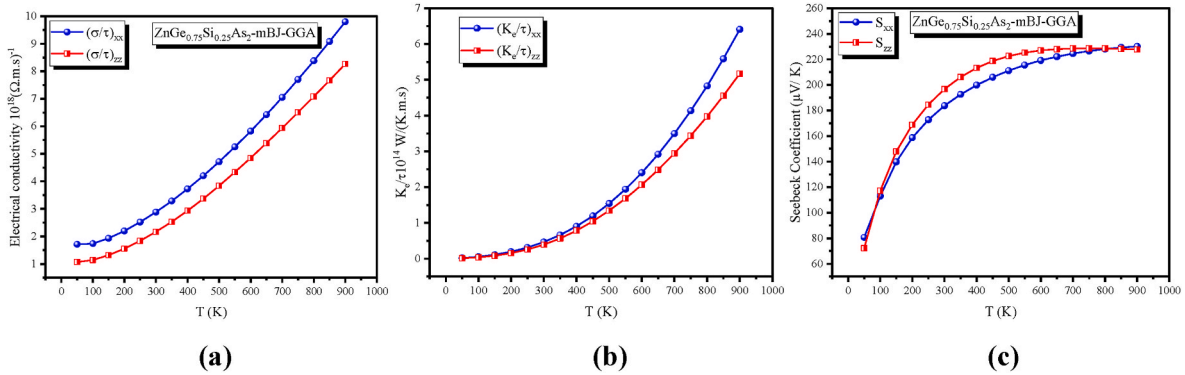

Fig. 7. Temperature dependence of the electrical conductivity, thermal conductivity and Seebeck coefficient for $ZnGe_{1-x}Si_xAs_2$ at (x = 0, 0.25, 0.5, 0.75 and 1) alloys in both directions (xx) and (zz).

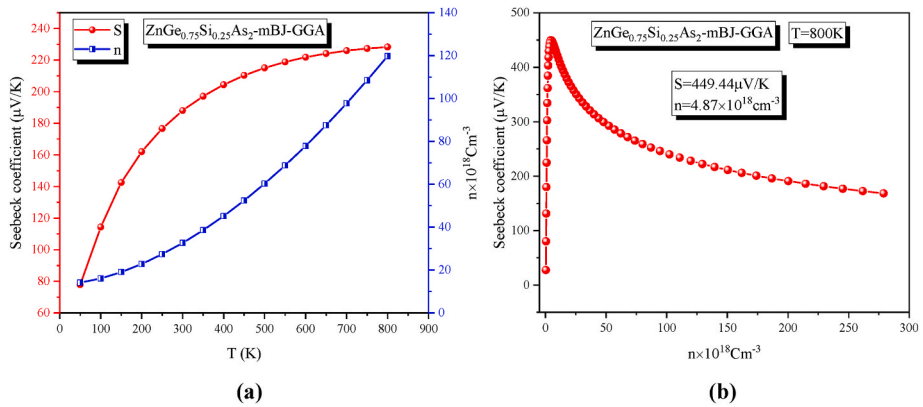

Fig. 8. The Seebeck coefficient of $ZnGe_{0.75}Si_{0.25}As_2$ as function of the temperature and carrier concentrations.

concentration on the Seebeck coefficient at T = 800 K. Fig. (8b) shows that the highest value of S is 449.44 μV/K, which is attained by reducing the charge carrier concentration to $n = 4.87 \times 10^{18}$ cm^{-3}.

4. Conclusions

In this study, we employed the first-principles full-potential linearized augmented plane wave (FP-LAPW) method, as implemented in the WIEN2k code, to systematically investigate the effects of silicon (Si) substitution on the structural, electronic, optical, and thermoelectric properties of the $ZnGeAs_2$ chalcopyrite semiconductor. The exchange-correlation potential was treated using LDA, GGA, and mBJ functionals to ensure a comprehensive analysis of the material properties.

4.1. Structural and electronic properties

Our calculations for the ground-state properties of $ZnGeAs_2$ and $ZnSiAs_2$, using the GGA functional, demonstrate good agreement with both experimental measurements and previous theoretical results, validating the accuracy of our computational approach. Alloying Ge with Si in the $ZnGe_{1-x}Si_xAs_2$ alloys introduces subtle changes in lattice parameters, reflecting the ionic radii differences and bonding characteristics between Ge and Si. Importantly, the electronic band structure analysis reveals that all $ZnGe_{1-x}Si_xAs_2$ alloys ($0 \leq x \leq 1$) exhibit a direct band gap at the Γ-Γ point, which is particularly advantageous for optoelectronic applications, such as light-emitting diodes (LEDs) and laser diodes, where efficient light emission is crucial. Additionally, we find that alloying shifts the band gap energies, offering tunability for specific optoelectronic requirements.

5. Optical properties

The optical properties of the $ZnGe_{1-x}Si_xAs_2$ alloys were investigated by analyzing the complex dielectric function $\varepsilon(\omega)$, including both the real $\varepsilon_1(\omega)$ and imaginary $\varepsilon_2(\omega)$ parts. The results reveal that the alloys exhibit anisotropic optical behavior and high absorption coefficients in the energy range of 1.5–6.5 eV, suitable for applications in optoelectronic devices. Substitution of Ge with Si significantly impacts optical performance, as exemplified by $ZnGe_{0.25}Si_{0.75}As_2$, which shows the highest refractive index and the most substantial energy loss. The high reflectivity observed in the ultraviolet region (13.5 eV) suggests the potential use of these alloys as effective UV radiation shields. The ability to tailor optical properties through silicon alloying highlights the novelty of this study and broadens the material's potential for various optical applications, including photovoltaics and UV protection.

6. Thermoelectric properties

The thermoelectric properties of the $ZnGe_{1-x}Si_xAs_2$ alloys were explored using the BoltzTraP code. Our results confirm that these alloys are p-type semiconductors, as evidenced by positive Seebeck coefficients. Importantly, alloying Ge with Si significantly enhances thermoelectric performance, as seen in $ZnGe_{0.75}Si_{0.25}As_2$, which exhibits a maximum Seebeck coefficient of 228.26 μV/K at 800 K. This composition also demonstrates the tunability of thermoelectric properties through carrier concentration optimization, with the Seebeck coefficient reaching 449.44 μV/K at $n = 4.87 \times 10^{18}$ cm^{-3}. These results underline the critical role of alloying in optimizing thermoelectric performance for energy conversion and thermal management applications.

7. Significance and future directions

This study provides novel insights into the role of alloying in tailoring the structural, electronic, optical, and thermoelectric properties of $ZnGe_{1-x}Si_xAs_2$ chalcopyrite alloys. The findings demonstrate the potential of silicon substitution to achieve tunable material properties, including band gap energies, optical behavior, and thermoelectric performance. Such tunability enables these materials to be optimized for specific applications, such as light-emitting diodes, photovoltaics, thermoelectric power generation, and UV protection.

Future research should focus on experimental validation of these theoretical predictions and the development of advanced synthesis techniques to produce high-quality alloys. Additionally, exploring the effects of alternative dopants and alloying elements could further expand the range of tunable properties and enhance device performance. This study not only contributes to a deeper understanding of $ZnGe_{1-x}Si_xAs_2$ alloys but also establishes a foundation for future advancements in optoelectronic and thermoelectric applications, demonstrating the transformative impact of alloying strategies in chalcopyrite semiconductors.

CRediT authorship contribution statement

S. Bougaa: Writing – original draft, Investigation, Conceptualization. **H. Baaziz:** Writing – review & editing, Writing – original draft, Supervision, Software, Investigation. **T. Ghellab:** Methodology, Investigation, Data curation. **S. Adalla:** Visualization, Resources, Data curation. **L. Bouhdjer:** Visualization, Resources, Data curation. **Ş. Uğur:** Resources, Methodology, Data curation. **G. Uğur:** Methodology, Investigation, Formal analysis. **Z. Charifi:** Validation, Software, Methodology, Data curation.

Declaration of competing interest

The authors declare that they have no known competing financial interests or personal relationships that could have appeared to influence the work reported in this paper.

Data availability

Data will be made available on request.

References

[1] B.R. Pamplin, T. Kiyosawa, K. Masumoto, Prog. Cryst. Growth Char. 1 (1979) 331.
[2] S.N. Rashkeev, S. Limpijumnong, W.R.L. Lambrecht, Phys. Rev. B 59 (1999) 2737.
[3] V. Kumar, A.K. Shrivastava, V. Jha, J. Phys. Chem. Solid. 71 (2010) 1513.
[4] J.L. Shay, J.H. Wernick, in: Ternary Chalcopyrite Semiconductors: Growth, Electronic Properties, and Applications, first ed., Pergamon Press, Oxford, New York, 1975.
[5] V. Kumar, S.K. Tripathy, V. Jha, Appl. Phys. Lett. 101 (2012) 192105.
[6] B. Xu, H. Han, J. Sun, L. Yi, Phys. B Condens. Matter 404 (2009) 1326.
[7] J. Drahokoupil, I. Drbohlav, J. Harák, M. Polčík, A. Šimůnek, Solid State Commun. 103 (1997) 303.
[8] G.S. Solomon, J.B. Posthill, M.L. Timmons, MRS Proc. 144 (1988) 61.
[9] S.I. Shah, J.E. Greene, Mater. Lett. 2 (1983) 115.
[10] K. Masumoto, S. Isomura, W. Goto, J. Phys. Chem. Solid. 27 (1966) 1939.
[11] A. Gaur, K. Khan, U. Ahuja, J. Sahariya, A. Soni, Optoelectronic Investigations of ZnGeAs2: A First Principle TB-mBJ Approximation, 2020 030368. Jodhpur, India.
[12] F. Boukabrine, F. Chiker, H. Khachai, A. Haddou, N. Baki, R. Khenata, B. Abbar, A. Khalfi, Phys. B Condens. Matter 406 (2011) 169.
[13] S. Sahin, Y.O. Ciftci, K. Colakoglu, N. Korozlu, J. Alloys Compd. 529 (2012) 1.
[14] I.V. Fedorchenko, A.V. Kochura, S.F. Marenkin, A.N. Aronov, L.I. Koroleva, L. Kilanski, R. Szymczak, W. Dobrowolski, S. Ivanenko, E. Lahderanta, IEEE trans. Magn 48 (2012) 1581.
[15] A.V. Krivosheeva, V.L. Shaposhnikov, V.E. Borisenko, J. Lazzari, Phys. Status Solidi 251 (2014) 1007.
[16] R. Mouacher, T. Seddik, B. Rezini, B.U. Haq, M. Batouche, G. Uğur, S. Uğur, A. Belfedal, J. Solid State Chem. 309 (2022) 122996.
[17] G.K.H. Madsen, P. Blaha, K. Schwarz, E. Sjöstedt, L. Nordström, Phys. Rev. B 64 (2001) 195134.
[18] P. Blaha, K. Schwarz, F. Tran, R. Laskowski, G.K.H. Madsen, L.D. Marks, J. Chem. Phys. 152 (2020) 074101.
[19] J.P. Perdew, Y. Wang, Phys. Rev. B 45 (1992) 13244.
[20] J.P. Perdew, A. Ruzsinszky, G.I. Csonka, O.A. Vydrov, G.E. Scuseria, L. A. Constantin, X. Zhou, K. Burke, Phys. Rev. Lett. 100 (2008) 136406.
[21] A.D. Becke, E.R. Johnson, J. Chem. Phys. 124 (2006) 221101.
[22] G.K.H. Madsen, D.J. Singh, Comput. Phys. Commun. 175 (2006) 67.
[23] P. Hohenberg, W. Kohn, Phys. Rev. 136 (1964) B864.
[24] W. Kohn, L.J. Sham, Phys. Rev. 140 (1965) A1133.
[25] T.J. Scheidemantel, C. Ambrosch-Draxl, T. Thonhauser, J.V. Badding, J.O. Sofo, Phys. Rev. B 68 (2003) 125210.
[26] T. Thonhauser, T.J. Scheidemantel, J.O. Sofo, J.V. Badding, G.D. Mahan, Phys. Rev. B 68 (2003) 085201.
[27] F.D. Murnaghan, Proc. Natl. Acad. Sci. U. S. A 30 (1944) 244.
[28] H. Salehi, E. Gordanian, Mater. Sci. Semicond. Process. 47 (2016) 51.
[29] Q.-B. Meng, C.-Y. Xiao, Z.-J. Wu, K. Feng, Z.-D. Lin, S.-Y. Zhang, Solid State Commun. 107 (1998) 369.
[30] M. Levalois, G. Allais, Phys. Status Solidi 109 (1988) 111 (a).
[31] S. Sharma, A.S. Verma, Eur. Phys. J. B 87 (2014) 159.
[32] A.G. Norman, J.M. Olson, M.J. Romero, M.M. Al-Jassim, Electron Microscopy Studies of Potential 1-eV Bandgap Semiconductor Compounds ZnGeAs2 and Zn3As2 Grown by MOVPE: Preprint, 2001.
[33] F.W. Scholl, E.S. Cory, Mater. Res. Bull. 9 (1974) 1511.
[34] S.I. Shah, J.E. Greene, J. Crystal Growth 68 (1984) 537.
[35] S.K. Tripathy, V. Kumar, Ab-Initio Calculation of ZnGeAs2 Semiconductor, Thapar University, Patiala, Punjab, India, 2014, pp. 1084–1086.
[36] B.-H. Jeong, M. Jeong, Y. Song, K. Park, J.-S. Park, Crystals 11 (2021) 883.
[37] A. Janotti, S.-H. Wei, S.B. Zhang, S. Kurtz, Phys. Rev. B 63 (2001) 195210.
[38] H.S. Saini, M. Singh, A.H. Reshak, M.K. Kashyap, J. Alloys Compd. 518 (2012) 74.
[39] A. Yu, Valov, N.A. Goryunova, E.I. Leonov, V.M. Orlov, Acta Physica 33 (1973) 1.
[40] C.H.L. Goodman, Nature 179 (1957) 828.
[41] H.A. Kramers, London, Edinburgh Dublin Phil. Mag. J. Sci. 46 (1923) 836.
[42] S. Adachi, Properties of Semiconductor Alloys: Group-IV, III-V and II-VI Semiconductors, Wiley, Chichester, U.K, 2009.
[43] G. Tse, D. Yu, Comput. Condens. Matter 4 (2015) 59.
[44] A.H. Reshak, Z.A. Alahmed, S. Azam, Int. J. Electrochem. Sci. 9 (2014) 975.
[45] M. Hassan, N.A. Noor, Q. Mahmood, B. Amin, Curr. Appl. Phys. 16 (2016) 1473.
[46] M.S. Yaseen, G. Murtaza, R.M. Arif Khalil, Curr. Appl. Phys. 18 (2018) 1113.
[47] S. Tab, A. Boudali, M. Berber, M. Driss Khodja, O.L. El Hachemi, H. Moujri, Appl. Phys. A 126 (2020) 544.
[48] S.J. Montiel-Perales, C. Guarneros-Aguilar, M. Boujnah, F. Caballero-Briones, Phys. B Condens. Matter 687 (2024) 416087.
[49] A. Yadav, P. Deshmukh, K. Roberts, N. Jisrawi, S. Valluri, J. Phys. Commun. 3 (2019) 105001.
[50] S. Ohta, T. Nomura, H. Ohta, K. Koumoto, J. Appl. Phys. 97 (2005) 034106.
[51] P. Govindaraj, K. Murugan, K. Venugopal, Mater. Chem. Phys. 295 (2023) 127190.
[52] B. Chelluri, T.Y. Chang, A. Ourmazd, A.H. Dayem, J.L. Zyskind, A. Srivastava, J. Cryst. Growth 81 (1987) 530.